RSC Advances

This is an *Accepted Manuscript*, which has been through the Royal Society of Chemistry peer review process and has been accepted for publication.

Accepted Manuscripts are published online shortly after acceptance, before technical editing, formatting and proof reading. Using this free service, authors can make their results available to the community, in citable form, before we publish the edited article. This *Accepted Manuscript* will be replaced by the edited, formatted and paginated article as soon as this is available.

You can find more information about *Accepted Manuscripts* in the **Information for Authors**.

Please note that technical editing may introduce minor changes to the text and/or graphics, which may alter content. The journal's standard **Terms & Conditions** and the **Ethical guidelines** still apply. In no event shall the Royal Society of Chemistry be held responsible for any errors or omissions in this *Accepted Manuscript* or any consequences arising from the use of any information it contains.

Journal Name

ARTICLE

Engineered cation vacancy plane responsible for the reduction in lattice thermal conductivity and improvement in thermoelectric property of Ga_2Te_3 based semiconductors

Dingqi Tian[a,b], Haiyun Liu[a], Yuan Deng[c]*, Zhengliang Du[b], Jiaolin Cui[b]*

Based on the inherent Ga vacancies in Ga_2Te_3, we use the preferential occupation of Cu in the Ga lattice, which can be confirmed by calculating the formation energy and refining Rietveld, to disturb the vacancy path, and thereby have cleverly manipulated of the vacancy plane. At the meantime we revealed that the sample annealed for 30 days has generated Heaven rain-shaped discontinuous vacancy planes which can effectively reduce the lattice thermal conductivity (k_L) and increase the bandgap (E_g), thus accounting for the remarkable improvement in thermoelectric performance. However, with the annealing time extending from 30 days to 95 days, there is a gradual enhancement in k_L and limited improvement in thermoelectric property, which is caused by the amalgamation or restructuring of the discontinuously vacancy planes.

1. Introduction

Thermoelectric (TE) performance can be characterized by the dimensionless figure of merit, ZT, $ZT=\alpha^2\sigma T/\kappa$, where T is absolute temperature, α is the Seebeck coefficient, σ is the electrical conductivity and κ is the thermal conductivity mainly consisting of electronic (κ_e) and lattice (κ_L) components. In order to enhance the ZT value, we should increase the power factor p, $p=\alpha^2\sigma$, and simultaneously reduce the κ value. Because of the low σ value of the materials[1,2], it is usually the lattice component (κ_L) predominates in many wide gap semiconductors rather than electronic part (κ_e). Hence, how to reduce the total κ comes down to the issue of how to effectively reduce the κ_L. In recent years, the nanostructuring technique [3] has been successfully applied in many TE materials such as Bi_2Te_3- and PbTe based alloys with narrow bandgaps. The lattice part (κ_L) has been reduced remarkably, as the nanostructure in the materials decreases phonon mean free path and introduces scattering events.[4,5] However, for the wide gap Ga_2Te_3 semiconductor ($E_g=1.65eV$ [6,7], ~1.0eV [8,9]) we need to further explore the nanostructuring concept and use more effective approach to reducing the lattice part κ_L.

Ga_2Te_3 has an ordered vacancy sphalerite structure.[10] In each domain in Ga_2Te_3 threre are two thirds of ordered Ga atoms occupying the $4c$ Wyckoff positions (1/4, 1/4, 1/4), while the remaining one third of $4c$ positions are vacancies (shown in Fig.1[10,11]), where the layers denoted A, B and C stack up in the
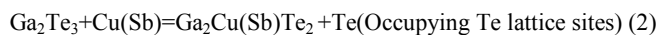
<111> direction. Te atoms in Ga_2Te_3 are settled in $4b$ site (0,0,0). From layer A to the next layer B, one vacant site on A is followed by a vacant site on B, then by another one on C. This arrangement of the vacant site generates a vacancy path within the domain and periodic vacancy planes within a single grain.[2,12,13] The vacancy path will discontinue at the domain boundary, and there will be a new path starting in a new domain. Since the inherent vacancies are essential to blocking the transports of phonons and carriers, therefore, the intrinsic Ga_2Te_3 has poor electrical conductivity ($<10^3\Omega^{-1}m^{-1}$ at 850K) and low lattice κ_L (<0.5 $WK^{-1}m^{-1}$ at 850K).[2]

If a foreign element occupies the Ga vacancy site, the vacant paths will be disturbed In that case, we are able to apply external energy to change the sites of substituted atoms and Ga vacancies, and thereby create a space that is big enough for us to engineer the disturbed vacancy paths (planes). The vacancy paths disturbance might lead to a direct evolution of the microstructure. Under such circumstance, the phonon transport path will alter, and the lattice thermal conductivity and TE performance can thus be tuned.[14]

2. Results and Discussion

The X-ray diffraction patterns for different annealing samples are shown in Fig.S1, and no visible impurity phases, such as GaTe and Ga_2Te_5 which can easily forme in the Ga_2Te_3 based alloy systems when T cools down (elevates) to 850 °C (407 °C),[10] have been identified. This indicates that the elements Cu and Sb have been incorporated into the Ga_2Te_3 crystal lattice, either as substituted atoms settling in the Ga and Te lattice sites, or as interstitial atoms

getting into the lattice structure. In order to confirm the preferential occupation of Cu in the Ga_2Te_3 lattice sites, we have calculated the formation energies when Cu (Sb) occupies the lattice or enters the intercalating sites in Ga_2Te_3, and the site occupations of Cu (Sb) using Rietveld refinement based on the X-ray diffraction data. The formation energies were calculated according to the following reactions:

$$Ga_2Te_3+Cu(Sb)=GaCu(Sb)Te_3+Ga(\text{Occupying Ga lattice sites}) \quad (1)$$

$$Ga_2Te_3+Cu(Sb)=Ga_2Cu(Sb)Te_2+Te(\text{Occupying Te lattice sites}) \quad (2)$$

$$Ga_2Te_3+Cu(Sb)=Ga_2Cu(Sb)Te_3 \qquad (\text{Settling as an interstice}) \quad (3)$$

Then, it is given that:

$$E_f = E_f (GaCu(Sb)Te_3)+E_T(Ga)-E_T(Ga_2Te_3)-E_T(Cu(Sb)) \quad (4)$$

$$E_f=E_f(Ga_2Cu(Sb)Te_2)+E_T(Te)-E_T(Ga_2Te_3)-E_T(Cu(Sb)) \quad (5)$$

$$E_f=E_f(Ga_2Cu(Sb)Te_3)-E_T(Ga_2Te_3)-E_T(Cu (Sb)) \quad (6)$$

Where E_f is the formation energy and E_T is the total energy of each material.

The results show that the formation energies (E_f) are -0.72 eV, 1.31eV or 3.76eV, respectively, as Cu occupies the Ga, Te lattice sites or as an interstitial atom. If it is the case of Sb, the E_f values are 4.96eV, 0.78eV or 9.21eV. Suggesting that Cu (Sb) preferentially occupies the Ga (Te) lattice sites, rather than the interstitial ones.

The Rietveld refinement, based on the following models (A, B, C and D), also reveals that Cu and Sb are preferentially settled in the Ga and Te sites, respectively, see Table 1 and Fig.2.

for model A,
$$SOF(Cu)_{4b}+SOF(Sb)_{4b}+SOF(Te)_{4b}=1 \quad (7)$$
$$SOF(Cu)_{4c}+SOF(Sb)_{4c}+SOF(Ga)_{4c}=2/3 \quad (8)$$
for model B,
$$SOF(Cu)_{4b}+SOF(Sb)_{4b}+ SOF(Ga)_{4b}+ SOF(Te)_{4b}=1 \quad (9)$$
$$SOF(Cu)_{4c}+SOF(Sb)_{4c}+SOF(Ga)_{4c}+ SOF(Te)_{4c}=2/3 \quad (10)$$
for model C,
$$SOF(Cu)_{4b}+SOF(Sb)_{4b}+ SOF(Ga)_{4b}+ SOF(Te)_{4b}=1 \quad (11)$$
$$SOF(Cu)_{4c}+SOF(Sb)_{4c}+SOF(Ga)_{4c}=2/3 \quad (12)$$
for model D,
$$SOF(Cu)_{4b}+SOF(Sb)_{4b}+SOF(Te)_{4b}=1 \quad (13)$$
$$SOF(Cu)_{4c}+SOF(Sb)_{4c}+SOF(Ga)_{4c}+ SOF(Te)_{4c}=2/3 \quad (14)$$

The preferential settling of Cu in the Ga sites is actually plausible as Cu^+ has a larger ironic radius (0.77Å) than Ga^{3+} (0.62 Å), and it is thus more energetically favorable in the Ga sites.[15,16] Since Cu^+ tends to occupy Ga sites, the concentration of the Ga vacancy decreases with the Cu^+ concentration increasing in the cation sublattice. Such a change is just like the situation where Cd and Hg are incorporated into the III–VI compounds.[17]

Fig.3a–d exhibits the high–resolution TEM images of four samples (these four samples were denominated as S–10, S–30, S–60 and S–95, corresponding to their annealings at 390 ^oC for 10 days, 30 days, 60 days and 95 days respectively), which indicate the restructuring process of the vacancy path (plane) within the Ga_2Te_3 through different annealings. From the images, we observed that S–10 exhibits conventional polycrystalline structure consisting of many nano–domains with different orientations (Shown in Fig.3(a), where the SAED pattern as an insert was indexed on the *F*-43*m* structure of Ga_2Te_3. In the meantime, S–30 has generated nano strips like Heaven rain with an identical orientation on (111) plane (Shown in Fig.3(b), where an insert is the FT diagram). These nano strips, which are less than 5 nm in length but are randomly distributed within the grain, should be the partially–formed discontinuous vacancy planes. When the sample was subjected to 60 days' annealing, the image obtained shows a picture of relatively regularly shaped zigzag domains at (111) plane (see Fig.3(c), where the insert is the FT diagram). These domains are probably wrapped by vacancy planes with different sizes that might be amalgamated from the Heaven rain–shaped vacancy planes in S–30 (see Fig.3(b)). In S–95 we observed many small randomly distributed parallelogram–shaped nano domains (circled by white dotted lines), and some faintly visible zigzag–shaped ones (see Fig.3(d)). Some cells of parallelogram–shaped nano domains projected on (110) plane have a size of ~0.4 nm × 0.6 nm, which is comparable to the size of those in Ref.10. The energy diffraction spectrum (EDS) of the alloy is shown in Fig.S2. The restructuring of Ga vacancy plane above verifies the fact that when there is external energy, the Ga vacancies will act as point defects that favor the interdiffusion of Cu^+ ions and Ga vacancies, by changing the sites between Cu^+ and vacancies. It is the interdiffusion between Cu^+ and Ga vacancies that effectively engineer the vacancy paths (planes).

The engineered vacancy plane in Ga_2Te_3 based alloys alters the electron and phonon scattering mechanism, and it eventually tailors the TE performance. The results are shown in Fig.4a–d, where the S–30 gives higher α values (α_{max}=450.9μV/K at 636K, and 342.8μV/K at 734K) (Fig.4a), but has a relatively low electrical (σ) and thermal conductivities (κ_L) (σ=1.88×10^3 $\Omega^{-1}m^{-1}$, κ_L=0.37 $WK^{-1}m^{-1}$ at 734K) (Fig.4b,c). The insert in Fig.4c is the total κ, whose value is a function of the temperature. On the other hand, the S–60 shows relatively low α values (α_{max}=365.4 μV/K at 665K, and 251.5 μV/K at 734K) and high σ and κ_L (σ=3.59×10^3 $\Omega^{-1}m^{-1}$, κ_L=0.53 $WK^{-1}m^{-1}$ at 734K) (Fig.4b,c). Because the Seebeck coefficient is profoundly affected by both the scattering factor (γ) and carrier concentration (n), which, though enhancing with temperature, cancel out each other according to the relation: $\alpha=\gamma-\ln n$. That is why we firstly observed the increased α values with temperature until 640~660K, and then decreases. Besides, the lattice part κ_L of all the samples roughly obeys a T^{-1} relation, and it reduces with temperature, which suggests that the phonon scattering mechanism dominates over the measured temperature range. Combining three parameters (α, σ and κ) we attain the ZT values as a function of temperature, as shown in Fig.4d, where the S–30 gives the highest ZT value (ZT$_{max}$= 0.41 at 734K), and S–10 the lowest

(ZT_{max}= 0.25 at 734K). Although the ZT value is smaller than those reported in other wider gap semiconductors,[18] it is about 2.5 times that of undoped Ga_2Te_3 (ZT=0.16 at 850K).[2]

It is reported that ZT value is closely related to the bandgap, and a wider bandgap could increase the ZT value at high temperatures by inhibiting the formation of minority carriers of opposite sign.[19] Alloying lead chalcogenides with a wider band gap compound, such as $MgTe$[20] and $CdTe$,[21] provides an effective approach to this issue. Through measuring the band gap (E_g) in the present materials, we attain an E_g value of ~0.90eV for S−30 (see Fig.5), which is the largest among four samples. This figure is in good agreement with the estimated result using $E_g=2e\alpha_{max}T_{max}$, [22] where e is the electron charge, as shown in Table 2. The results in Fig.5 suggest that the Heaven rain−shaped vacancy planes that are discontinuously and randomly distributed have a wider bandgap, which leads to the highest α, lowest σ value[23] and highest ZT value.[19] In contrast, the relatively regular vacancy plane in S−60 gives a small bandgap (E_g=0.66eV), and hence has the lowest α and highest σ.

Although there is still not a direct correlation between the lattice part κ_L and the bandgap (E_g) yet in the present work, the gradual enhancement of the lattice part κ_L proves that a great change of the phonon relaxation time τ has been taking place as the annealing time increases from 30 to 95 days. In the present material system we only need to consider the scattering from point defects (τ_D), nanoparticles (τ_N), phase/grain boundaries (τ_B) and Umklapp process (τ_U),[24] Which is:

$$\tau^{-1} = \tau^{-1}_D + \tau^{-1}_N + \tau^{-1}_B + \tau^{-1}_U \qquad (15)$$

When the sample (S−10) is subjected to short time annealing, the phonon scattering resulted from the point defects predominates. However, in S−30 the generated Heaven rain−shaped vacancy planes with less than 5nm in length would lead to a large suppression of the phonon transport, which thereby reduces the τ_N and κ_L significantly.[25] With the annealing time extending, some discontinuous vacancy planes in S−30 amalgamate or restructures through interdiffusion of the Ga vacancies and Cu^+ ions, which decreases the phase/grain boundaries and yields the increase of τ_D, τ_N and τ_B. That is why we have observed relatively high κ_L values in S−60 and S−95.

3. Experimental Section

The ingots of $Ga_{1.9}Cu_{0.05}Sb_{0.1}Te_{2.95}$, consisting of four elements Cu, Ga, Sb and Te with the purity of 5N, were prepared in the four evacuated silica tubes. These four tubes were heated at 1100 °C for 24 h, and rapidly cooled down to 390 °C, and then maintained at this temperature for 10 days, 30 days, 60 days and 95 days each. In terms of the electronegativities between Cu (1.9) and Ga (1.81), Sb (2.05) and Te (2.1), the element Cu is likely to occupy the Ga lattice sites, while the Sb occupies the Te sites according to the preliminary experiments.[23] In this light, the designed material would be Ga−poor and Te−rich if such hypothesis is fully realized. This material, which is poor in Ga, will provide more Ga vacancy, and hence will leave much more space to engineer the vacancy plane with external energy. The amount of the element Te (2.95) is seen to higher than the maximum (2.9) because element Te is volatile and can easily evaporate during the experimental process. The electrical properties (α and σ) were measured using ZEM−2 apparatus and the data attained was confirmed for several times using different samples (the error was below 6% for α and 10% for σ). The thermal diffusivities and heat capacities were measured using TC−1200RH with the errors less than 12% and 6%. Therefore, the thermal conductivities (κ) at RT~735K were calculated as the products of material densities, thermal diffusivities and heat capacities. The lattice parts (κ_L) were attained through the subtraction of the electronic parts (κ_e) from the total κ, that is $\kappa_L=\kappa-\kappa_e$. The detailed experimental procedures for other parameters were reported elsewhere.[26]

Rietveld refinements of S−30 using XRPD were performed using FULLPROF, and X−ray diffraction peakshapes were quantified by a Pseudo-Voigt function and a Pseudo-Voigt function with the Finger-Cox-Jephcoat asymmetry correction, respectively. The background was described as a shifted Chebyschev type. The following parameters were refined: lattice parameters, peak shape parameters, atomic coordinates, isotropic displacement parameters (U_{iso}) and site occupation factors (SOFs). Each structural model was refined to convergence.

4. Conclusions

Through different annealing process we have successfully engineered inherent vacancy plane in Ga_2Te_3 via the preferential occupation of Cu in the Ga lattice sites, and observed the reduction in lattice thermal conductivity (κ_L) as well as the improvement of thermoelectric performance. After the sample has experienced a 30 days' annealing procedure, we have discovered a newly−formed discontinuous Heaven rain−shaped vacancy plane generated within the sample, and also obtained a dimensionless figure of merit (ZT) (0.41), which is about 2.5 times that of intrinsic Ga_2Te_3. However, with the annealing time extending, an amalgamation or restructure of the discontinuous vacancy planes occurs, which results in an enhancement in κ_L and limited improvement in thermoelectric performance.
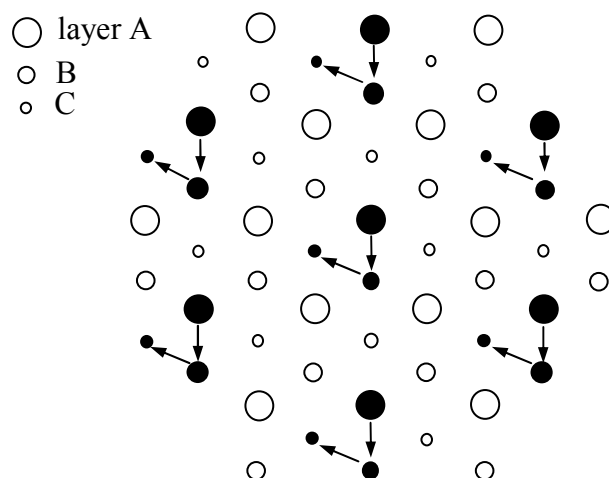
Figure 1 Projection (along <111>) of layers A,B,C in an ordered structure of Ga_2Te_3. Black circles denote vacancies. Only $4c$ (Ga) sites are represented.

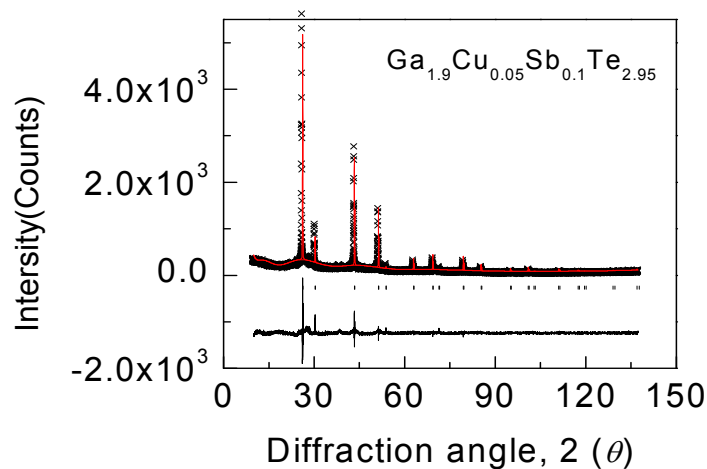Fig.2 Rietveld refinement using X-ray diffraction data for $Ga_{1.9}Cu_{0.05}Sb_{0.1}Te_{2.95}$ annealed for 30 days at 390^oC. Observed ($\times\times\times$) and calculated (solid line) X-ray powder diffraction patterns are shown.
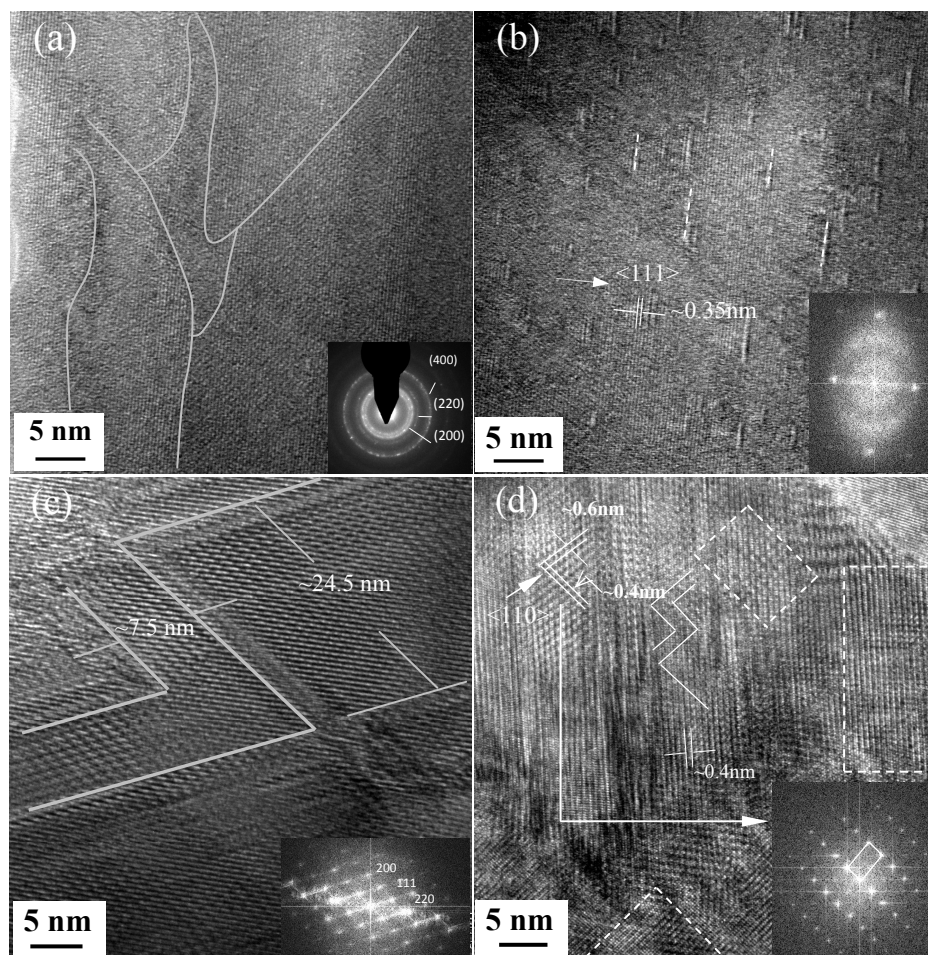
Figure 3 High–resolution TEM images of the samples annealed for different times.
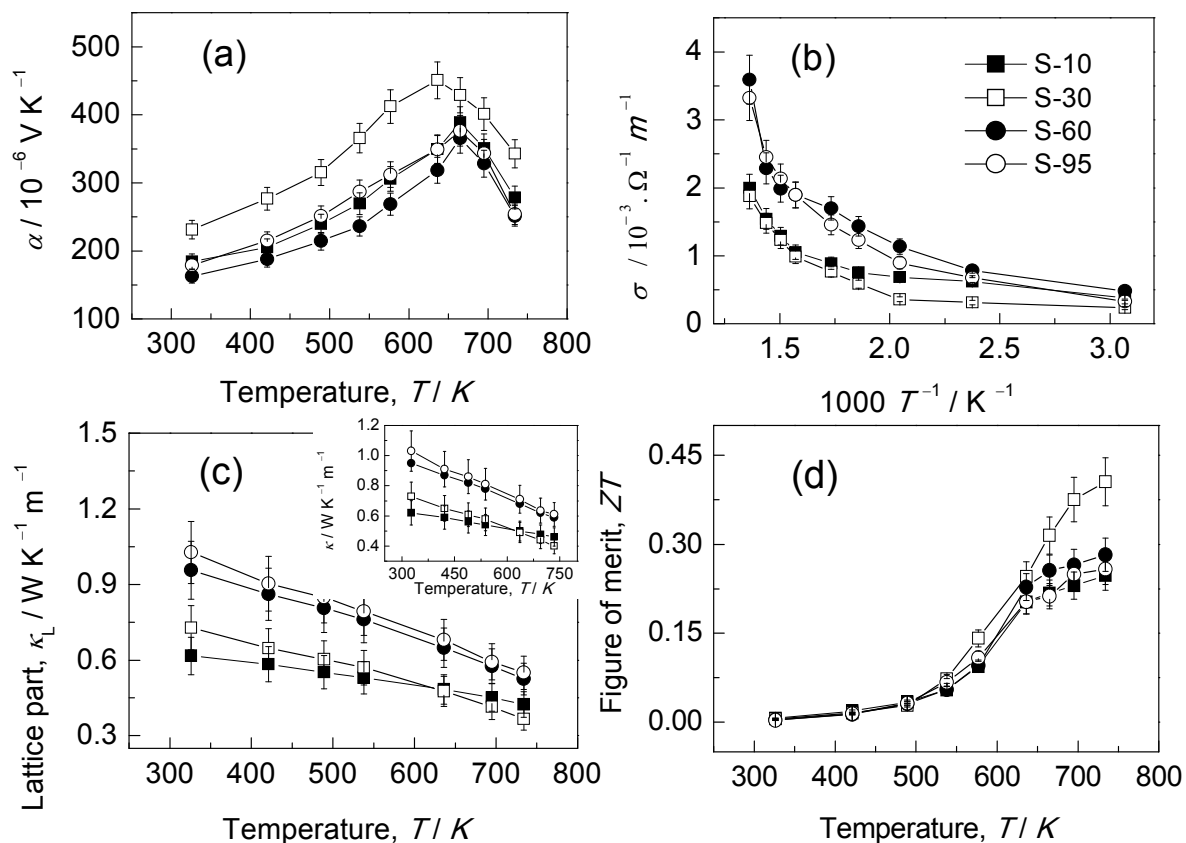(a) S–10, (b) S–30, (c) S–60, (d) S–95

Figure 4   Thermoelectric properties as a function of temperature for different samples, (a) Seebeck coefficients, (b) Electrical conductivities, (c) Lattice thermal conductivities, an insert is the total thermal conductivities, (d) Dimensionless TE figure of merit (ZT).
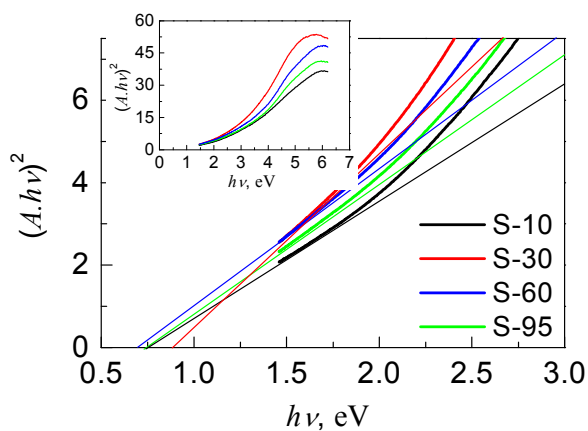

Figure 5   The relation between $(Ah\nu)^2$ for different samples, the upper right insert is the full spectra $(Ah\nu)^2$ $(h\nu)$.

Table 1 Structural parameters and refinement details for $Ga_{1.9}Cu_{0.05}Sb_{0.1}Te_{2.95}$ compounds annealed for 30 days by Rietveld refinements

Parameters	$Ga_{1.9}Cu_{0.05}Sb_{0.1}Te_{2.95}$			
	Model A	Model B	Model C	Model D
	Cation 4*b*			
SOF(Te)	0.8967	0.9000	0.9000	0.7816
SOF(Ga)		0.0034	0.0061	0
SOF(Cu)	0.0033	0.0071	0.0057	0.0118
SOF(Sb)	0.0997	0.0997	0.0943	0.1041
$100U_{iso}$ [Å^2]	2.4300	2.5780	2.9210	2.2290
	Cation 4*c*			
SOF(Te)		0.0002	0	–0.0005
SOF(Ga)	0.5680	0.6226	0.5657	0.6200
SOF(Cu)	0.0474	0.0936	0.0513	0.0474
SOF(Sb)	0.0052	0.0004	0.0054	0.0011
$100U_{iso}$ [Å^2]	2.4090	2.3840	2.4740	2.2390
	Reliability Factors			
χ^2	2.1240	2.1310	2.0560	2.0710
wR_p	0.1128	0.113	0.1111	0.1114
R_p	0.0879	0.0879	0.0867	0.0870

Model A: $(Te,Cu,Sb)_{4b}(Ga,Cu,Sb)_{4c}$

Model B: $(Te,Ga,Cu,Sb)_{4b}(Te,Ga,Cu,Sb)_{4c}$

Model C: $(Te,Ga,Cu,Sb)_{4b}(Ga,Cu,Sb)_{4c}$

Model D: $(Te,Cu,Sb)_{4b}(Te,Ga,Cu,Sb)_{4c}$

RSC Advances Accepted Manuscript

Table 2 Estimated and measured bandgaps for the samples with different annealing times

Samples	Estimated E_g, eV	Measured E_g, eV
10	0.82	0.75
30	0.92	0.90
60	0.77	0.66
95	0.79	0.75

Notes and references

[a] Materials Science and Engineering College, Taiyuan University of Technology, Taiyuan 030024, China

[b] Institute of Materials Engineering, School of Materials, Ningbo University of Technology, Ningbo 315016, China

[c] School of Chemistry & Environment, Beihang University, Beijing 100191, China.

†Corresponding author, J.L.Cui, E-mail: cuijiaolin@163.com.

Electronic Supplementary Information (ESI) available: [Supporting Information is available from the RSC Online Library or from the author.]. See DOI: 10.1039/b000000x/

RSC Advances Accepted Manuscript

References

1 J.L. Yao, N. J. Takas, M. L. Schliefert, D. S. Paprocki, P. E. R. Blanchard, H.Y. Gou, A.Mar, C. L. Exstrom, S. A. Darveau, P. F. P. Poudeu, J. A. Ai, *Phys Rev. B* 2011, **84**, 075203.

2 K. Kurosaki, H. Matsumoto, A. Charoenphakdee, S. Yamanaka, M. Ishimaru, Y. Hirotsu, *Appl. Phys. Lett*. 2008, **93**, 012101.

3 a) X. Yan , G. Joshi , W. Liu , Y. Lan , H. Wang , S. Lee , J. W. Simonson , S. J. Poon , T. M. Tritt , G.   Chen , Z. F. Ren, *Nano Lett.* 2011, **11** , 556; b) G. J. Snyder , E. S. Toberer , *Nat. Mater*. 2008, **7** , 105; c) M. S. Dresselhaus , G. Chen , M. Y. Tang , R. G. Yang , H. Lee , D. Z. Wang , Z. F. Ren , J. P. Fleurial , P. Gogna, *Adv. Mater.* 2007, **19**, 1043; d) A. I. Hochbaum , R. Chen , R. D. Delgado , W. Liang , E. C. Garnett , M. Najarian , A. Majumdar, P. Yang, *Nature* 2008, **451**, 163; e) C. J. Vineis , A. Shakouri , A. Majumdar, M. G. Kanatzidis, *Adv. Mater.* 2010, **22**, 3970; f) Vikas Varshney, Ajit K. Roy, Douglas S. Dudis, J. Lee, B. L. Farmer, *Nanoscale*, 2012, **4**, 5009.

4 B. Poudel, Q. Hao, Y. Ma, Y. Lan, A. Minnich, B. Yu, X. Yan, D. Wang, A. Muto, D. Vashaee, X. Chen, J. Liu, M. S. Dresselhaus, G. Chen, Z. Ren, *Science* 2008, **320**, 634.

5 K. Biswas, J. He, I. D. Blum, C-I Wu, T. P. Hogan, D. N. Seidman, V. P. Dravid, M. G. Kanatzidis, *Nature*, 2012, **489**, 414.

6 G. Guizzetti, F. Meloni, *Luglio-Agosto* 1982,**1D**, 503.

7 H. Zhu, J. Yin, Y. Xia, Z. Liu, *Appl.Phys. Lett*. 2010, **97**, 083504.

8 K. Wuyts, J. Watté, G. Langouche, R. E. Silverans, G. Zégbé, J. C. Jumas, *J. Appl. Phys*. 1992, **71**, 744.

9 B. R. Pamplin, in *CRC Handbook of Chemistry and Physics*, 62nd ed.; edited by R. C. Weast and M. .I. Astle (CRC, Boca Raton, FL, 1982), pp. E-99-E-103.

10 M. Guymont, A. Tomas, M. Guittard, *Philos. Mag*. A 1992, **66**, 133.

11 E. Finkman, J.Tauc, *Phys. Rev. Lett*., 1973, **31**, 890.

12 a) C. E. Kim, K. Kurosaki, M. Ishimaru, H.Muta, S.Yamanaka, *J. Electron. Mater*. 2011, **40**, 999; b) H. Yang, D. T. Morelli, *J. Electron. Mater*. 2012, **41**,1270; c) S.Yamanaka, M. Ishimaru, A. Charoenphakdee, H. Matsumoto, K. Kurosaki, *J. Electron. Mater*. 2009, **38**, 1392; d) C.E. Kim, K. Kurosaki, M. Ishimaru, D.y. Jung, H. Muta, S. Yamanaka, *Phys. Status Solidi RRL* 2009, **3**, 221.

13. Y. Nakamura, N. Otsuka, *Appl. Phys. Lett*., 1991,**59**, 568.

14. Y. Liu, L. Chen, J. Li, *Acta Mater*. 2014, **65**, 308.

15 J.S. Rhyee, E. Cho, K.H. Lee, S.M. Lee, H.S. Kim, Y.S. Kwon, *J. Appl. Phys*. 2010, **107**, 053705.

16 C.H. de Groot, J.S. Moodera, *J. Appl. Phys*. 2001, **89**, 4336.

17 H. V. Wensierski, D. Weitze, V Leute, *Solid State Ionics* 1997, **101-103**, 479.

18 a) X. Y. Shi, F. Q. Huang, M. L. Liu, L.D. Chen, *Appl. Phys. Lett*. 2009, **94**, 122103; b) M. L. Liu, I. W. Chen, F. Q. Huang, L.D. Chen, *Adv. Mater*. 2009, **21**, 3808.

19 a) Y. Pei , H. Wang, G. J. Snyder, *Adv. Mater.* 2012, **24**, 6125; b) Y. Pei , A. D. LaLonde , N. A. Heinz , X. Shi , S. Iwanaga , H. Wang, L. Chen, G. J. Snyder, *Adv. Mater.* 2011, **23**, 5674; c) Y. Pei , N. A. Heinz , G. J. Snyder, *J. Mater. Chem.* 2011, **21**, 18256.

20 a) L. M. Rogers , A. J. Crocker , *J. Phys. D: Appl. Phys.* 1971, **4**, 1016 ; b) A. J. Crocker , B. J. Sealy , *J. Phys. Chem. Solids* 1972,**33**, 2183; c) L. Rogers , A. Crocker, *J. Phys. D: Appl. Phys.* 1972, **5**, 1671.

21 a) A. J. Crocker , L. M. Rogers, *J. Phys. Colloq.* 1968, **29**, C4 129; b) Y. Kulvitit , S. Rolland , R. Granger, C. M. Pelletier, *Rev. Phys. Appl*. 1980, **15**, 1501; c) L. M. Rogers, A. J. Crocker, *J. Phys. D: Appl. Phys*. 1971, **4**, 1006; d) A. Szot , A. Szczerbakow, K. Dybko, L. Kowalczyk, E. Smajek, V. Domukhovski, *Acta Phys. Pol., A* 2009, **116**, 959; e) P. Nikolic, *J. Phys. D: Appl. Phys*. **1966**, **17**, 341.

22 H.J. Goldsmid, J.W. Sharp, *J. Electron. Mater*. 1999, **28**, 869.

23 J.L. Cui, Y.L. Gao, H. Zhou, Y.P. Li, Q.S. Meng, J.F. Yang, *Appl. Phys. Lett.* 2012, **101**, 081908.

24 a) Y. Luo, J. Yang, G. Li , M. Liu, Y. Xiao, L. Fu, W. Li, P. Zhu, J. Peng, S. Gao, J. Zhang, *Adv. Energy Mater.* 2014, **4**, 1300599; b) M. Liu, X.Y. Qin, *Appl. Phys. Lett.* 2012, **101**, 132103; c) M. Liu, X. Y. Qin, C. S. Liu, Z. Zeng, *Appl. Phys. Lett.* 2011, **99**, 062112; d) H. Y. Lv, H. J. Liu, X. J. Tan, L. Pan, Y. W. Wen, J. Shi, X. F. Tang, *Nanoscale*, 2012, **4**, 511.

25 H. S. Shin, S. G. Jeon, J. Yu, Y.S. Kim, H. M. Parka, J. Y. Song, *Nanoscale*, 2014, printed

26 a) J. L. Cui, X. L. Liu, X. J. Zhang, Y. Y. Li, Y. Deng, *J. Appl. Phys.* 2011, **110**, 023708; b) J.L. Cui, Y.Y. Li, Y. Deng, Q.S. Meng, Y.L.Gao, H. Zhou, Y.P. Li, *Intermetallics* 2012, **31**, 217.